ADVANCED
MATERIALS

Supporting Information

for *Adv. Mater.*, DOI: 10.1002/adma.201801773

Defect-Enhanced Charge Separation and Transfer within Protection Layer/Semiconductor Structure of Photoanodes

Jianyun Zheng, Yanhong Lyu, Chao Xie, Ruilun Wang, Li Tao, Haibo Wu, Huaijuan Zhou, Sanping Jiang, and Shuangyin Wang**

Supporting Information

Defect-enhanced charge separation and transfer within protection layer/ semiconductor structure of photoanodes

Jianyun Zheng, Yanhong Lyu, Chao Xie, Ruilun Wang, Li Tao, Haibo Wu, Huaijuan Zhou, Sanping Jiang, and Shuangyin Wang**

Sample preparation

A 500-μm-thick, phosphorus-doped, single-side-polished, (100)-oriented, n-type Si wafer with a resistivity of 0.05– 0.2 Ω·cm was first cleaned sequentially in an ultrasonic bath of acetone, ethanol and distilled (DI) water for 20 min. Black Si was fabricated by metal-catalyzed electroless etching method. The clean wafer was immersed in a piranha solution (1:3 (v/v), 30 wt% H_2O_2:H_2SO_4) for 5 min and then in a 5 wt% HF for 10 min to remove the native SiO_2 layer. Subsequently, the wafer was rinsed with DI water and dipped in a mixed solution of 2 mM $AgNO_3$ and 2 wt% HF for 30 s. After that, the wafer was quickly rinsed with DI water again and transferred into the etching solution, which contained 40 wt% HF, 20 wt% H_2O_2 and DI water with a volume ratio of 3:1:10 for 150 s. After rinsing with DI water, the etched wafer was immersed in 40 wt% HNO_3 solution for 20 min to remove the Ag nanoparticle residue. Finally, the prepared wafer with porous surface (black Si) was rinsed with DI water and dried by air blowing.

Thin Ni metal layer was deposited on black Si and cleaned BK7 glass slides by using a direct current MS (dcMS) system (Chuangshiweina Co. Ltd., MSP-3200) to sputter planar round metal Ni target (purity > 99.5 wt%) in pure Ar (99.99%) atmosphere at room temperature by the power of 100 W. Subsequently, NiO_x layer without and with Nb doping was deposited on Ni metal layer by sputtering Ni target and Nb_2O_5 target (purity > 99.5 wt%) in mixed Ar/O_2 (99.99%) atmosphere. To obtain the different doping concentrations of Nb, the power charged on Nb_2O_5 target was 0, 30 and 90 W corresponding to NiO_x/Ni/black Si (labeled as NS), low Nb-doped NiO_x/Ni/black Si (labeled as *l*-Nb:NS) and high Nb-doped NiO_x/Ni/black Si (labeled as *h*-Nb:NS), respectively. After deposition, the fresh samples were treated by N_2 plasma under the working pressure of ~4.0 Pa for 30 min with radio frequency powers of 200 and 300 W, respectively. To make it easy to quickly state the samples, NS, *l*-Nb:NS and *h*-Nb:NS treated at 200 W or 300 W were denoted as NS_P_2, *l*-Nb:NS_P_2 and *h*-Nb:NS_P_2 or NS_P_3, *l*-Nb:NS_P_3 and *h*-Nb:NS_P_3, respectively.

The back sides of all samples were first polished, and then were coated by Pd layer with ~300 nm thickness and connected to a metal Cu wire, forming an ohmic back contact. Silver paint was applied to affix the Cu belt. After drying, the entire back side and partial front side of the black Si electrodes were encapsulated in epoxy, establishing an exposed active area of ~0.1 cm^2. Calibrated digital images and ImageJ were used to determine the geometrical area of the exposed electrode surface defined by epoxy.

Physicochemical characterization

To investigate the crystalline structure of the samples, a Rigaku diffractometer (Rigaku Ultima IV) using Cu Kα radiation (λ = 0.15406 nm) was employed to performing 2θ X-ray diffraction (XRD) scans with the grazing angle of 1° at the scan rate of $2°\cdot min^{-1}$. Raman measurement was carried out using a HR800 Raman microscope instrument with 532 nm Ar ion laser and a resolution of 1 cm^{-1}. The surface morphology of the film was obtained by an atomic force microscope (AFM, SII Nano Technology Ltd., Nanonavi Π) with noncontact mode. Aiming to determine the microstructure and composition of the film, field emission scanning electron microscopy (FESEM) with energy dispersive x-ray spectroscopy (EDS) was employed to observe the surface and cross section of the film. The chemical composition of the sample was analyzed by X-ray photoelectron spectroscopy (XPS, Thermo escalab 250XI) with monochromated Al Kα radiation on at a pass energy of 29.4 eV. All binding energies were referenced to the C1s peak (284.8 eV) arising from adventitious carbon. The atomic force microscopy (AFM) images presenting both the surface morphology, microscopic current-voltage (*I-V*) curves and current mapping images (at 10 V) were collected using a Nanocute SII scanning probe microscopy operated in contact and electric models. Photoluminescence (PL) spectra were measured at room temperature on a fluorescence spectrophotometer (Fls–980, Edinburgh) with an excitation wavelength of 405 nm. Time-resolved PL decay spectra were measured using a fluorescence lifetime spectrometer (Fls–980). The PL lifetime of all the samples were calculated by fitting the experimental decay transient data with bi-exponential decay model. To determine the concentration and species of oxygen defects of the samples, electron paramagnetic resonance (EPR) spectra were taken on a JES FA–200 (JEOL) continuous-wave EPR spectrometer by applying an X band (9.2 GHz) and a sweeping magnetic field at -50 °C. Additionally, EPR spectra of the samples without and with illumination were implemented at 0 °C by xenon lamp. To compare the EPR intensity reasonably and fairly, the mass of all the samples was normalized in EPR data.

The optical transmittance characteristics were monitored on a UV-visible-near-IR spectrophotometer (Hitachi, UV-4100) at normal incidence from 350 to 2600 nm. The absorption coefficient *a* relates to the transmittance *T* and film thickness *d* as following:

$$a = -\frac{ln(T)}{d} \tag{1}$$

The optical energy band gap of the sample has been estimated by using the classical relation of optical absorption

$$ah\upsilon = B(h\upsilon - E_g)^m \tag{2}$$

where B, E_g and hν denote as the band tailing parameter, the optical band gap and the photon energy, respectively. The value of m should be taken as 0.5, a characteristic value for the direct allowed transition which dominates over the optical absorption.

Magnetization (M) versus applied magnetic field (H) at 25 °C was measured using a Quantum Design superconducting quantum interference device (SQUID) magnetometer. The applied magnetic field was perpendicular to the sample surface unless noted otherwise. Magnetization data of all samples have not been corrected for diamagnetism of the Si substrate. Typical net magnetic moments for the samples used in this study were on the order of 10^{-6} emu absolute, which should be approximately two orders of magnitude larger than the base sensitivity of the SQUID magnetometer.

Electrical measurements

Temperature dependent tunneling experiments were performed on the samples. Before measuring, each sample was cut into 5×5 mm^2 and then glued onto one quartz glass by conductive silver paint (Leitsilber 200). Part of dried silver paint on the glass, which was exposed to air, is functioned as one electrode, while another electrode is produced by dotted the silver paint with a diameter of ~160 μm on surface of each sample. Tungsten probes were used to contact a front and back collectors for dry measurements. The substrate bias was scanned from 0 to 2.0 V while monitoring the current density.

Current versus Voltage (I-V) curves were performed using a GPS150 probe station equipped with a HW-1616 constant temperature controller and a keithley 2400 digital source meter. The Xe lamp with AM 1.5G filter were used for illumination, and calibrated to AM 1.5 intensity (100 mW·cm^{-2}) through light power meter (PerfectLight Co. Ltd., PL-MW 200). Before the measurement of the light current, each sample was cut into 5×5 mm^2 and then glued onto one quartz glass by conductive silver paint (Leitsilber 200). Part of dried silver paint on the glass, which was exposed to air, is functioned as one electrode, while another electrode is produced by dotted the silver paint on surface of each sample. Tungsten probes were used to contact a front and back collectors for dry measurements. To obtain the light current, the voltage range was all set at 0.0 V ~3.0 V with or without irradiation.

PEC measurement

A three-electrode cell (that is, Si-based photocathode as the working electrode, Pt wire as the counter electrode and Ag/AgCl as the reference electrode) was implemented for PEC measurements in a PEC 1000 system (PerfectLight Co. Ltd.) with illumination of solar light (AM 1.5G, 100 mW·cm^{-2}) using a solar simulator (optical fiber source, FX300). Before each measurement, the solar simulator intensity was calibrated with a reference silicon solar cell and a readout meter for the solar simulator irradiance (PerfectLight Co. Ltd., PL-MW 200). Two kinds of electrolytes were used, including 1.0 M aqueous NaOH and phosphate buffer solution (pH = 7.0) with 1.0 M Na_2SO_3. Liner-sweep voltammetry (*J*-*V*) data without any iR compensation were collected using a CHI 630E electrochemical workstation with or without illuminating. For a typical *J*-*V* measurement, the voltage was swept linearly at a scan rate of 0.01 V·s^{-1}. Readings for Ag/AgCl were converted to RHE using the following relationship.

$$E(\mathrm{RHE}) = E(\mathrm{Ag/AgCl}) + 0.197\mathrm{V} + 0.059 \times \mathrm{pH} \tag{3}$$

The Mott-Schottky plots were acquired at a frequency of 10 KHz in 1.0 M NaOH solution by a CHI 660 potentiostat. The Mott-Schottky equation is shown below:

$$\frac{1}{C^2} = \frac{2}{q\varepsilon_s\varepsilon_0 A^2 N_D}(V - V_{fb} - {}^{kT}\!/_{q}) \tag{4}$$

C is capacitance, q the charge of an electron (1.60 × 10^{-19} C), ε_0 the vacuum permittivity (8.85 × 10^{-14} F·cm^{-1}), ε_s the permittivity of silicon (1.05 × 10^{-14} F·cm^{-1}), A the area of the sample, N_D the donor density, V the appied bias, V_{fb} the flat band voltage, k Boltzmann's constant (1.38 × 10^{-23} J·K^{-1}), and T the temperature (25 °C). The x-intercept of the Mott-Schottky plot was reached at the bias that needs to be applied to cause the bands to become flat. Also, the slope of the plot can be used to calculate the donor density of the electrode. The x-intercept plus kT/q (~0.025 V) equals the flat band voltage. The donor density (N_D) can be calculated using the equation:

$$N_D = \frac{2}{e\varepsilon\varepsilon_0}\left[\frac{\mathrm{d}(1/C^2)}{\mathrm{d}V}\right]^{-1} \tag{5}$$

where ε and $\left[\frac{\mathrm{d}(1/C^2)}{\mathrm{d}V}\right]$ are the dielectric constant of silicon (11.68) and the slope of the sharp increase from 0.75-0.95 V region. Thus, N_D for NS, NS_P_3, *l*-Nb:NS and *l*-Nb:NS_P_3 can be calculated to be 9.4×10^{18}, 9.5×10^{18}, 10.0×10^{18} and 3.2×10^{18} cm^{-3}, respectively. The barrier heights can then be obtained from the flat band voltage using V_n, the difference in energy between the Fermi level and the conduction band. Applying the measured N_D and the density of states in the conduction band (N_C) of 2.8×10^{19} cm^{-3}, V_n is calculated to be 0.056 eV for *l*-Nb:NS_P_3 through Equation 6

$$V_n = kT\ln\left(\frac{N_C}{N_D}\right) \tag{6}$$

Supplementary Figures

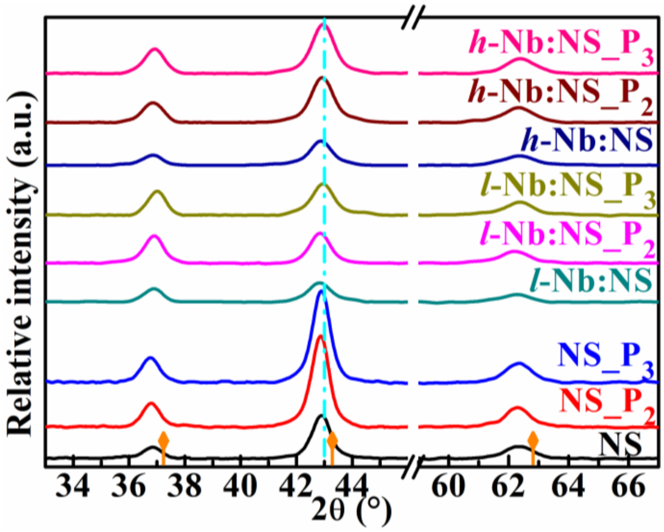

Figure S1. XRD patterns of the NiO_x-based/Ni/black Si photoanodes. The standard XRD pattern for NiO (orange rhombus) is shown at the bottom (JCPDS, No. 44-1159).

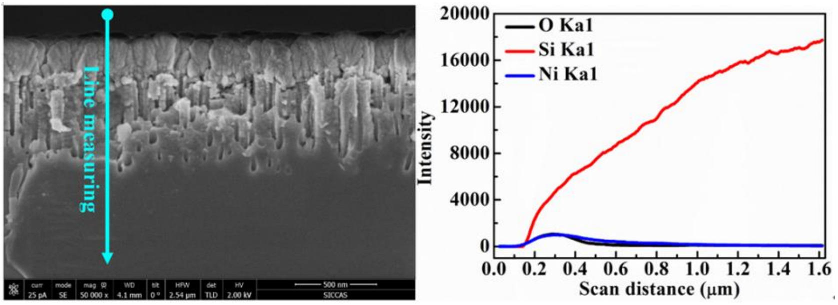

Figure S2. Cross-sectional FESEM images and corresponding EDS-line measurements for NS.

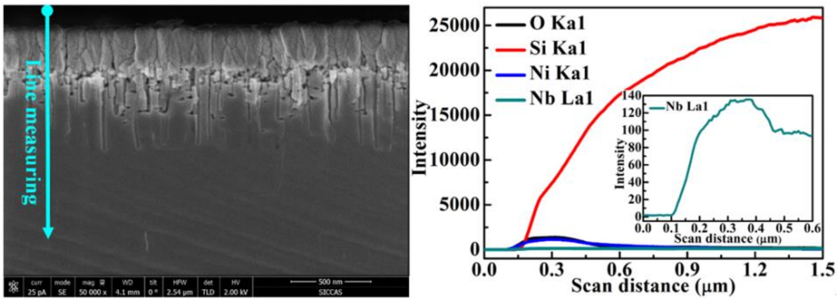

Figure S3. Cross-sectional FESEM images and corresponding EDS-line measurements for *l*-Nb:NS_P$_3$.

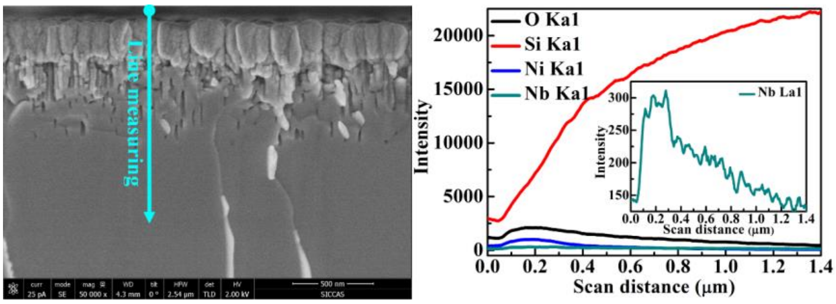

Figure S4. Cross-sectional FESEM images and corresponding EDS-line measurements for *h*-Nb:NS_P$_2$.

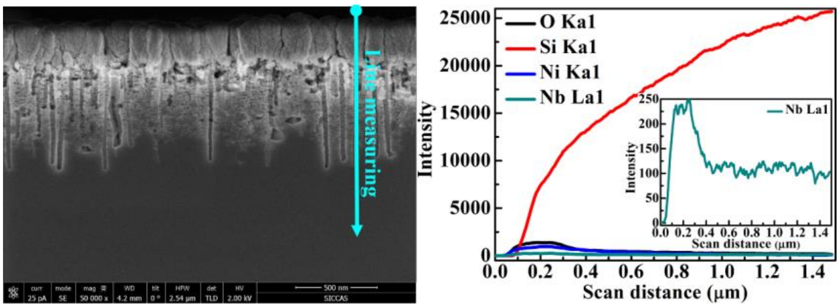

Figure S5. Cross-sectional FESEM images and corresponding EDS-line measurements for *h*-Nb:NS_P$_3$.

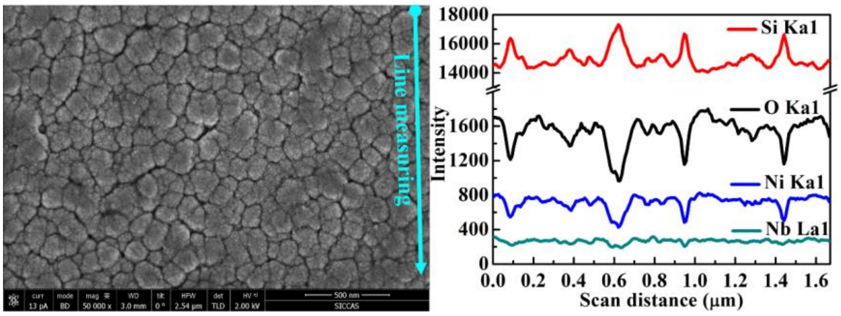

Figure S6. Top view FESEM images and corresponding EDS-line measurements for *h*-Nb:NS_P$_2$.

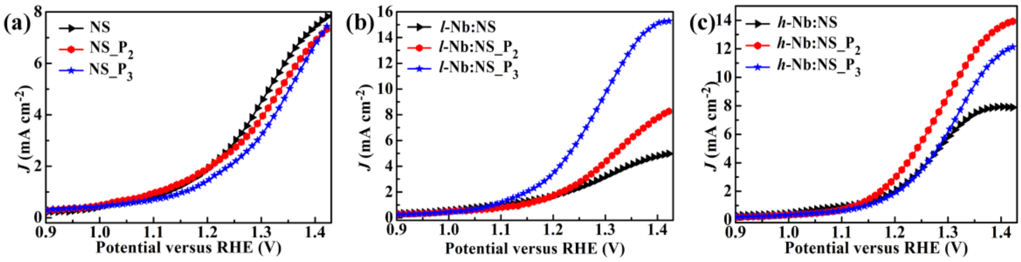

Figure S7. J-V curves of all the samples under one sun illumination in 1.0 M NaOH.

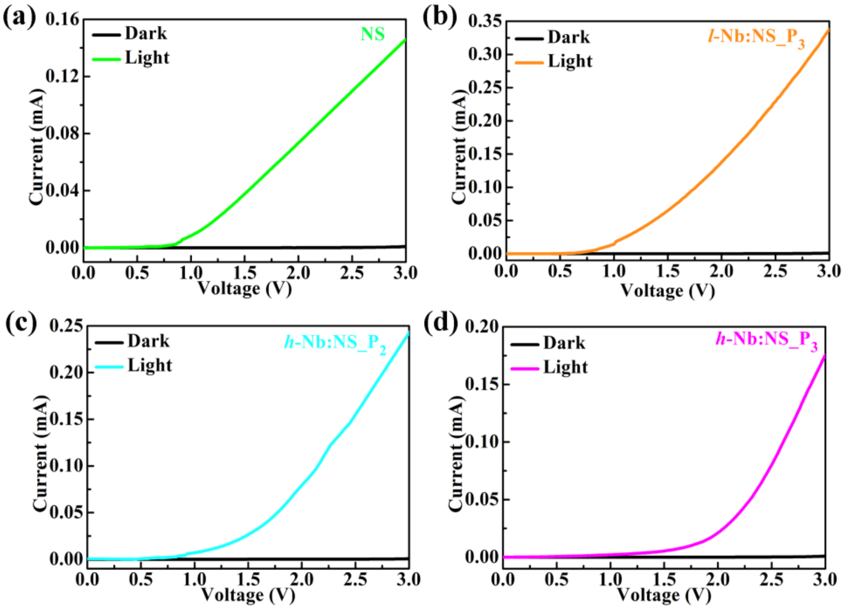

Figure S8. Dry current-potential (I-V) measurements under 100 mW·cm^{-2} white light illumination for one metal silver dot on the samples: (a) NS, (b) l-Nb:NS_P$_3$, (c) h-Nb:NS_P$_2$ and (d) h-Nb:NS_P$_3$.

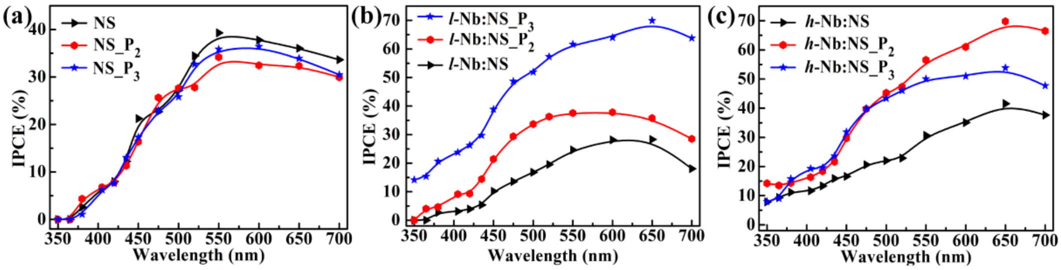

Figure S9. Incident photon-to-current efficiency (IPCE) of all the samples in 1.0 M NaOH at 1.43 V vs RHE.

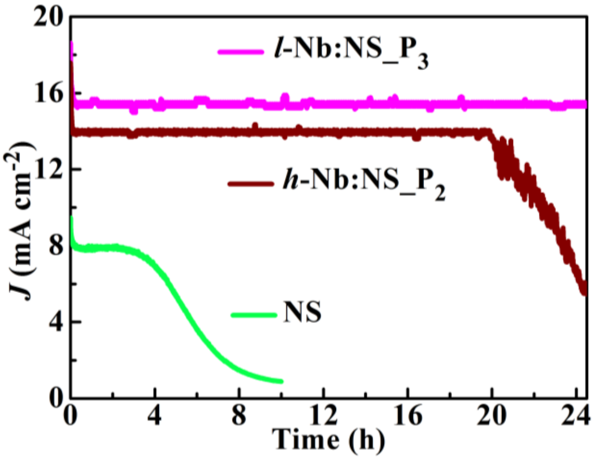

Figure S10. The durability experiments (*J*-*t*) of NS, *l*-Nb:NS_P$_3$ and *h*-Nb:NS_P$_2$ held at 1.43 V vs RHE in 1.0 M NaOH under 1 sun illumination.

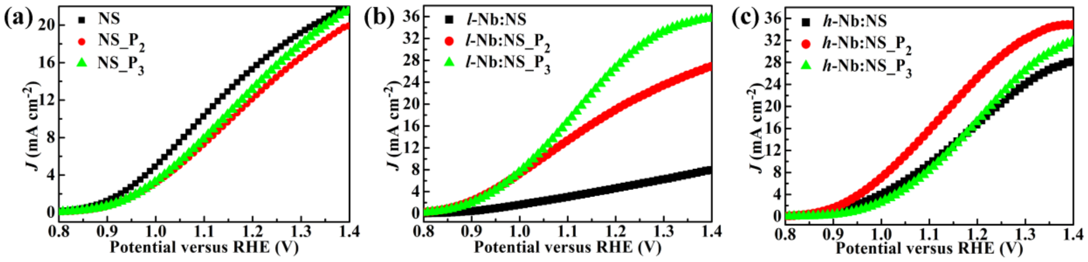

Figure S11. *J*-*V* curves of all the samples for sulfite oxidation measured in phosphate buffer (pH = 7.0) with 1.0 M Na_2SO_3 as the hole scavenger under one sun illumination.

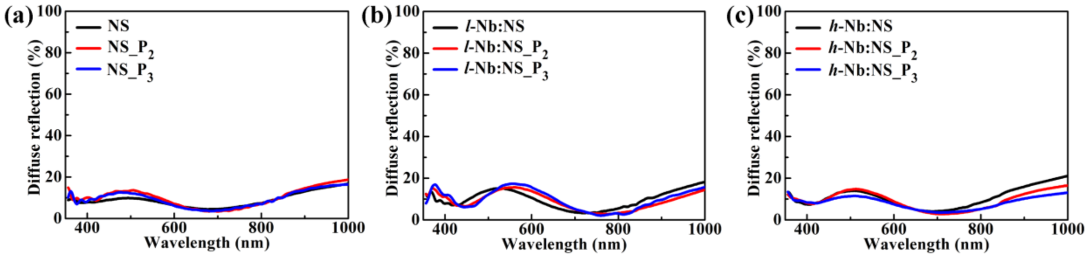

Figure S12. The measured total hemispherical optical reflectance of all the samples in air.

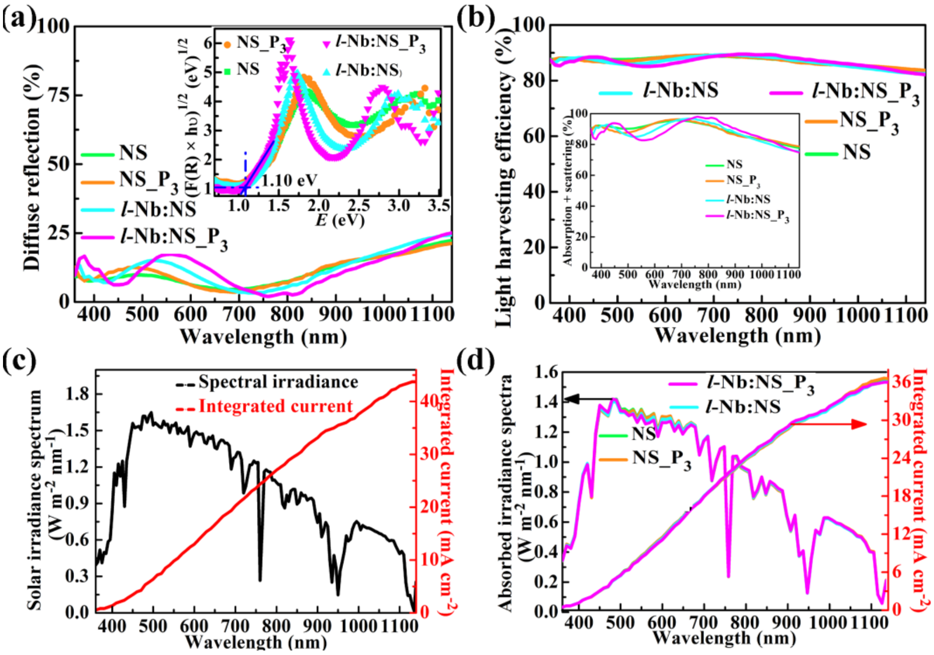

Figure S13. (a) The measured total hemispherical optical reflectance of NS, NS_P$_3$, *l*-Nb:NS and *l*-Nb:NS_P$_3$ in air. The inset shows the optical absorption coefficient as a function of the incident photon energy for indirect allowed transition for the samples. (b) The light harvesting efficiencies (η_{LHE}) of b-Si and BTBS2. η_{LHE} was calculated from the absorbance data (η_{ABS}) shown in the inset via the equation $\eta_{\mathrm{LHE}} = (1\text{-}10^{-\eta\mathrm{ABS}}) \times 100\%$. The inset is UV-visible absorption spectra of the samples derived from reflectance spectra through the relation absorption = 100 – transmittance – reflectance, assuming zero transmittance. (c) Irradiance and integrated current of AM 1.5G solar spectrum. (d) Absorbing solar irradiance spectra and integrated current of the samples. The absorbing solar irradiance spectra were the product of the AM 1.5G irradiance and η_{LHE}. Photocurrent density (J_{abs}) under 100% absorbed photon conversion efficiency can be estimated by the integrated current at the photoanodes across 350-1150 nm wavelength range.

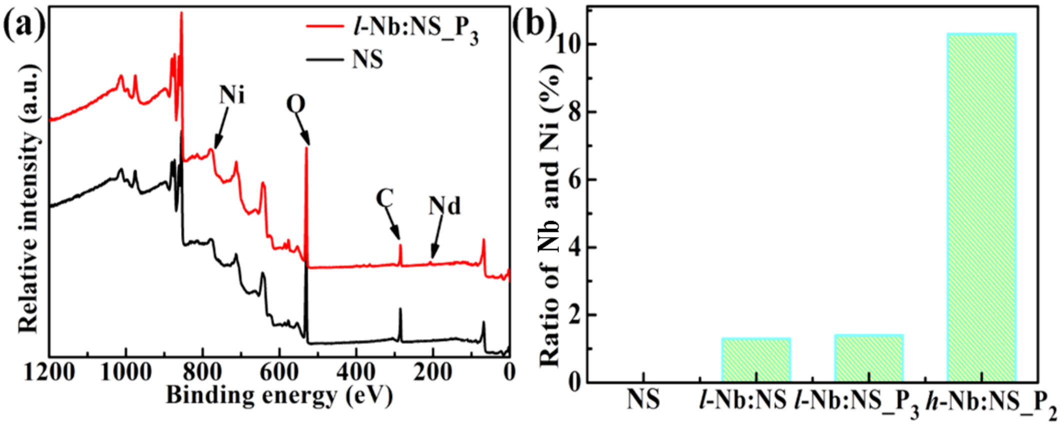

Figure S14. (a) XPS survey spectra of NS and *l*-Nb:NS_P$_3$. (b) Ratio of Nb and Ni of the samples on the surface. In Ni 2p spectra, an extra peak located at a binding energy of 861.3 eV or 861.5 eV was attributed to the satellite peak of Ni 2p$_{3/2}$.

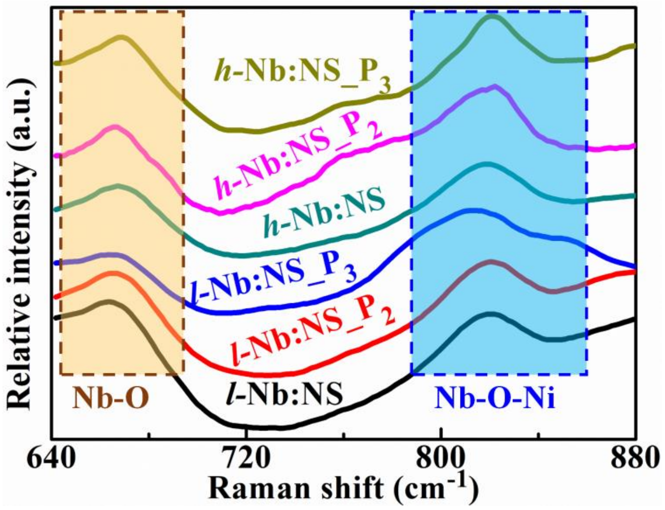

Figure S15. Raman spectra of *l*-Nb:NS, *l*-Nb:NS_P$_2$, *l*-Nb:NS_P$_3$, *h*-Nb:NS, *h*-Nb:NS_P$_2$ and *h*-Nb:NS_P$_3$. The brown and light blue rectangular boxes are marked as Nb-O mode and Nb-O-Ni mode, respectively.

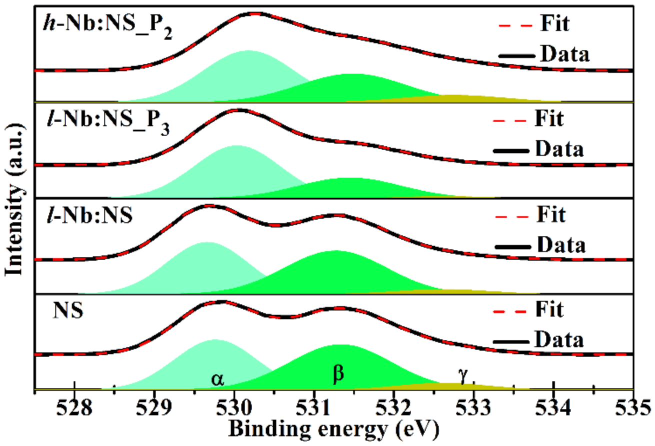

Figure S16. O 1s XPS spectra of NS, *l*-Nb:NS, *l*-Nb:NS_P$_3$ and *h*-Nb:NS_P$_2$. In detail, the peak at ~529.7 eV (Peak α) is assigned to the lattice oxygen, whereas the peak at ~531.3 eV (Peak β) is attributed to a high number of defect sites with lower oxygen coordination. The peak at ~532.6 eV (Peak γ) is associated with surface-adsorbed water molecules.

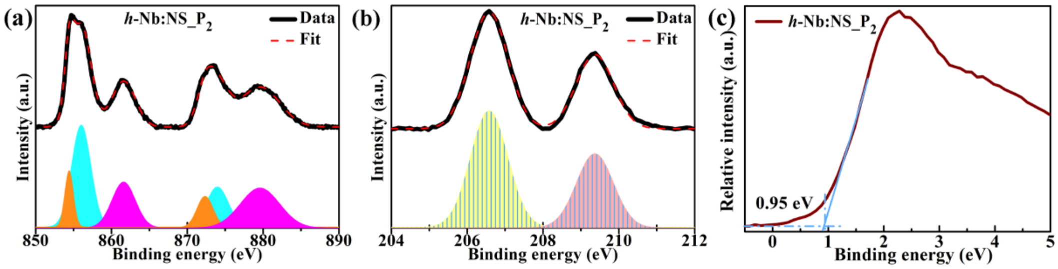

Figure S17. (a) Ni 2p XPS spectra of *h*-Nb:NS_P$_2$. The black solid lines are XPS data. The red dashed lines are the fitting of experimental data for the samples, which can be decomposed into a superposition of three peaks shown as orange (Ni^{2+}), light blue (Ni^{3+}), and pink (satellite peak). (b) Nb 3d XPS spectra of *h*-Nb:NS_P$_2$. (c) Valence-band XPS spectra of *h*-Nb:NS_P$_2$.

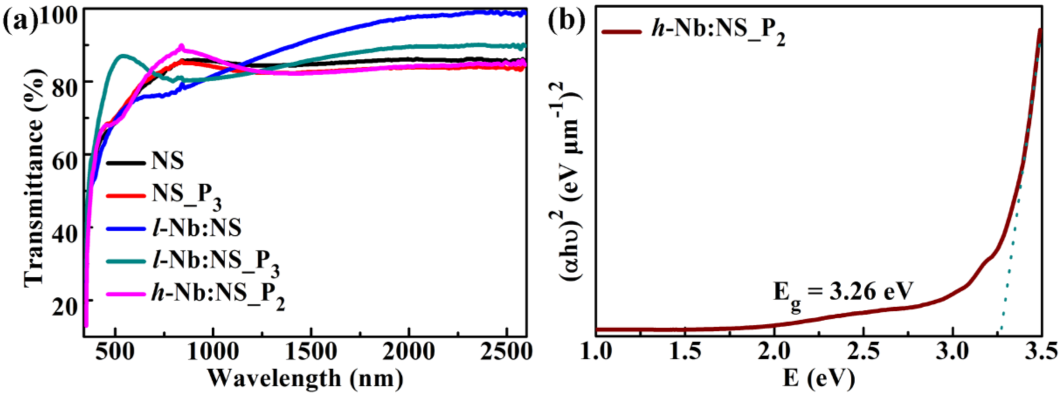

Figure S18. (a) UV-visible-near-IR transmittance spectra of the NiO$_x$-based layer deposited on BK7 wafer. (b) Optical absorption coefficients α as a function of the incident photon energy E for direct allowed transition for *h*-Nb:NS_P$_2$.

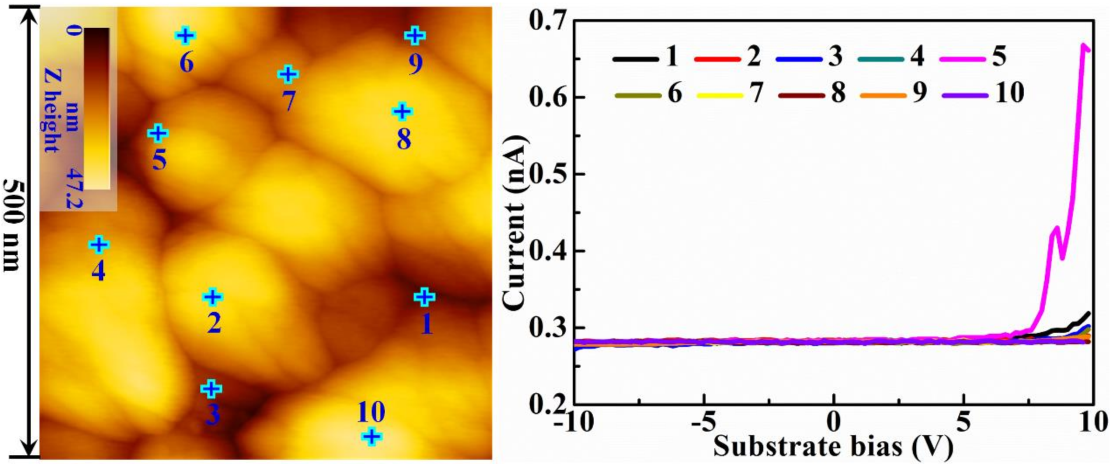

Figure S19. AFM topography image (left) and typical *I*-*V* curves of marked position by the number (right) for NS. Position 1-10 in AFM image corresponding to the colored *I*-*V* curve.

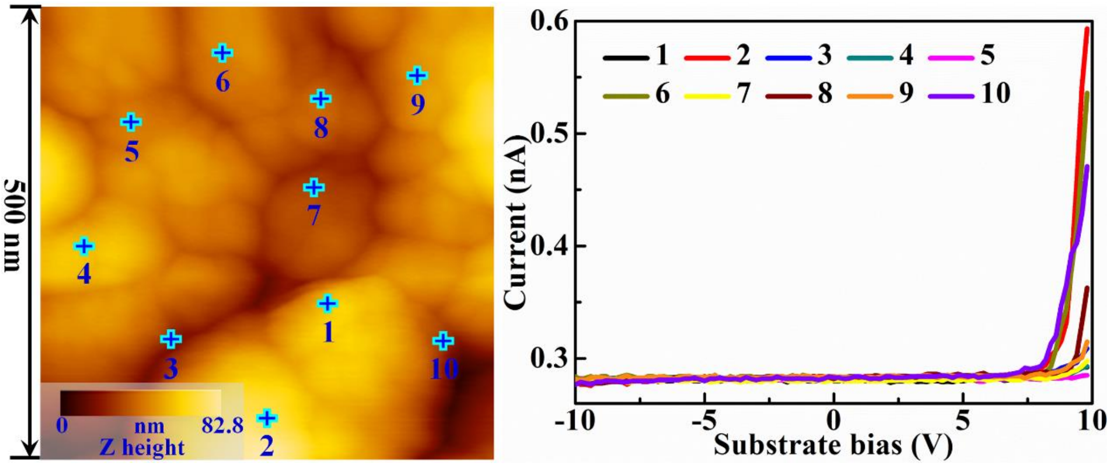

Figure S20. AFM topography image (left) and typical *I*-*V* curves of marked position by the number (right) for NS_P$_3$. Position 1-10 in AFM image corresponding to the colored *I*-*V* curve.

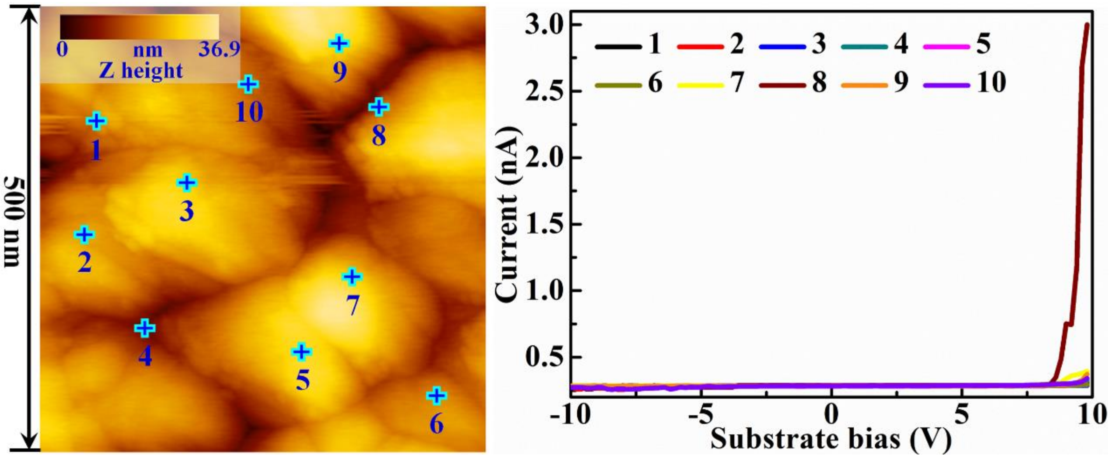

Figure S21. AFM topography image (left) and typical *I*-*V* curves of marked position by the number (right) for *l*-Nb:NS. Position 1-10 in AFM image corresponding to the colored *I*-*V* curve.

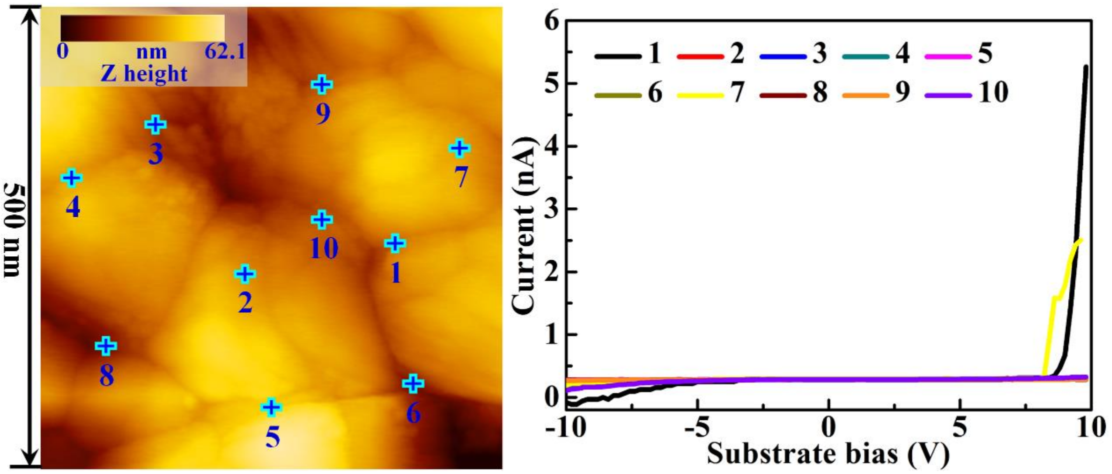

Figure S22. AFM topography image (left) and typical *I-V* curves of marked position by the number (right) for *h*-Nb:NS. Position 1-10 in AFM image corresponding to the colored *I-V* curve.

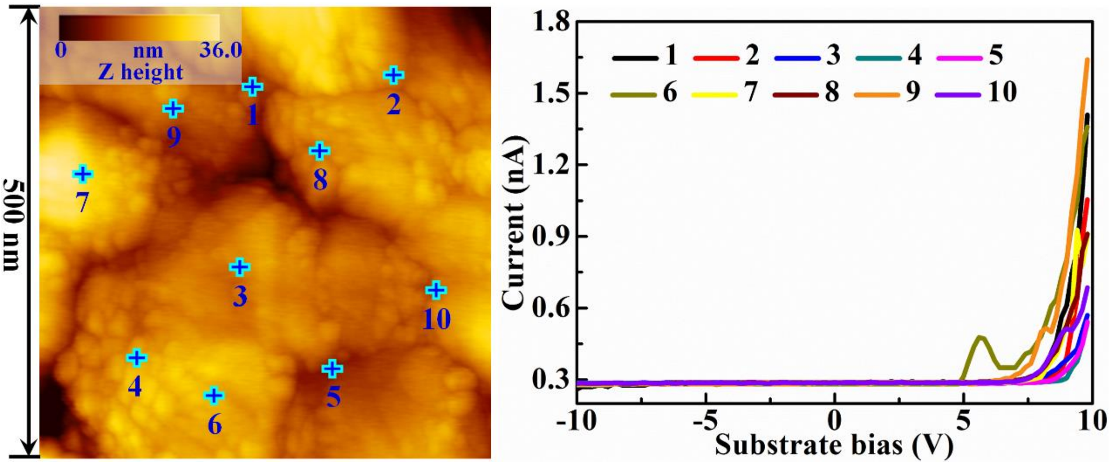

Figure S23. AFM topography image (left) and typical *I-V* curves of marked position by the number (right) for *h*-Nb:NS_P$_2$. Position 1-10 in AFM image corresponding to the colored *I-V* curve.

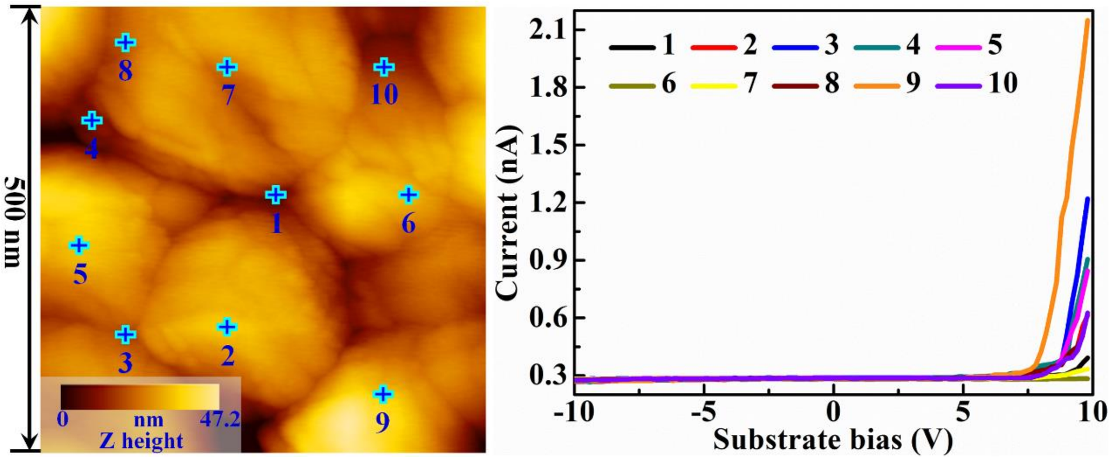

Figure S24. AFM topography image (left) and typical *I-V* curves of marked position by the number (right) for *h*-Nb:NS_P$_3$. Position 1-10 in AFM image corresponding to the colored *I-V* curve.

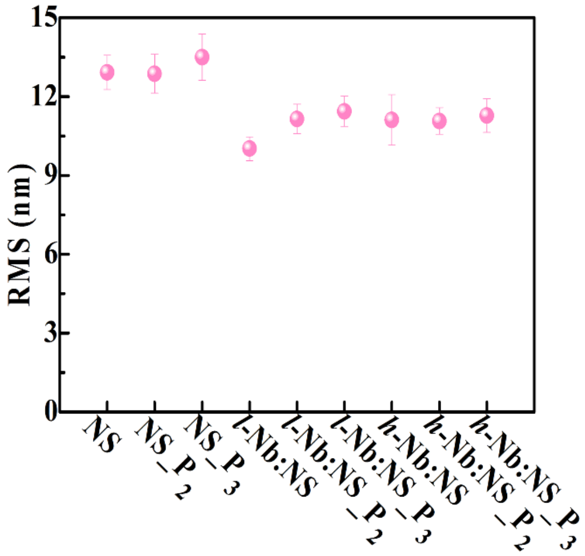

Figure S25. Root-mean-square (RMS) roughness of all the samples with 5× 5 μm^2 area.

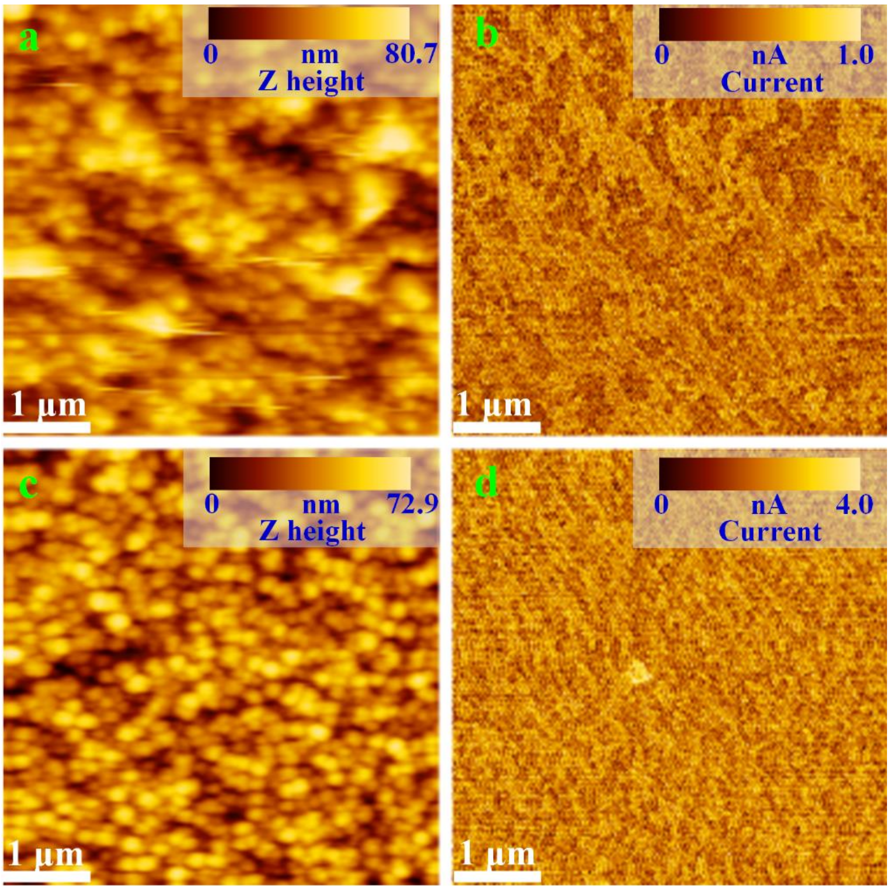

Figure S26. Topography *z*-height (left) and conductive AFM mapping (right) of NS (a and b) and *l*-Nb:NS_P$_3$ (c and d).

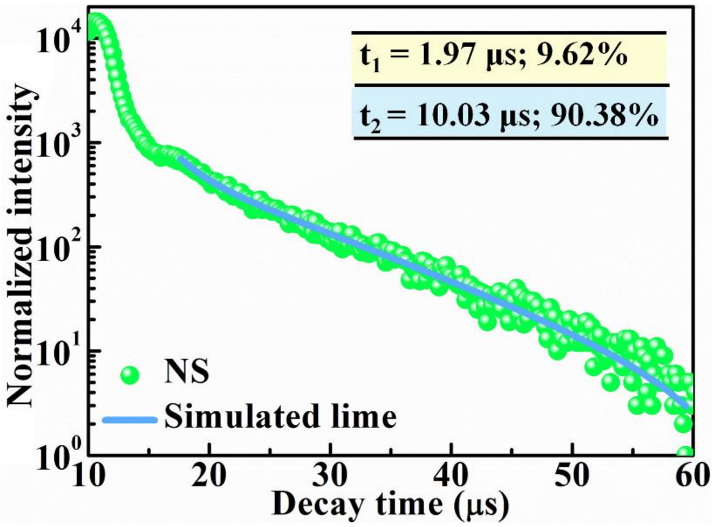

Figure S27. Time-resolved PL decay curve for NS at room temperature. Solid lines represent the kinetic fit using bi-exponential decay model. The inserted table provides the kinetics parameters of NS.

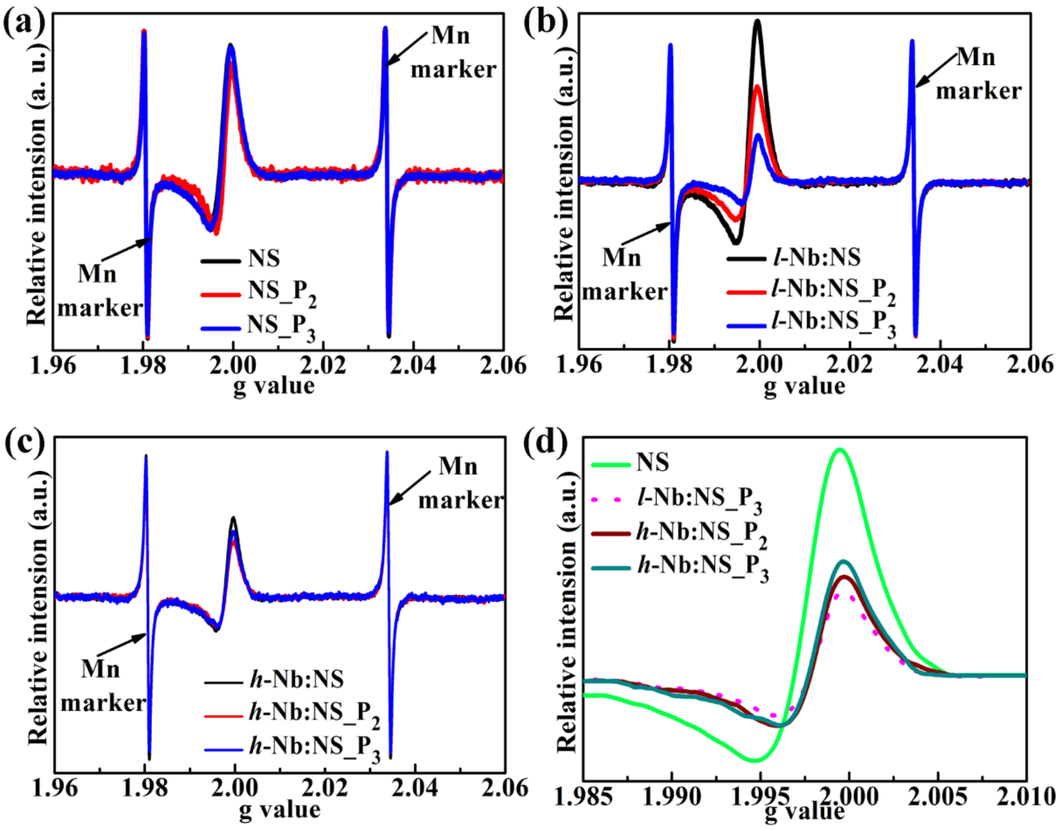

Figure S28. (a) EPR spectra of NS, NS_P_2 and NS_P_3 at -50 °C. (b) EPR spectra of *l*-Nb:NS, *l*-Nb:NS_P_2 and *l*-Nb:NS_P_3 at -50 °C. (c) EPR spectra of *h*-Nb:NS, *h*-Nb:NS_P_2 and *h*-Nb:NS_P_3 at -50 °C. (d) EPR spectra of NS, *l*-Nb:NS_P_3, *h*-Nb:NS_P_2 and *h*-Nb:NS_P_3 at -50 °C.

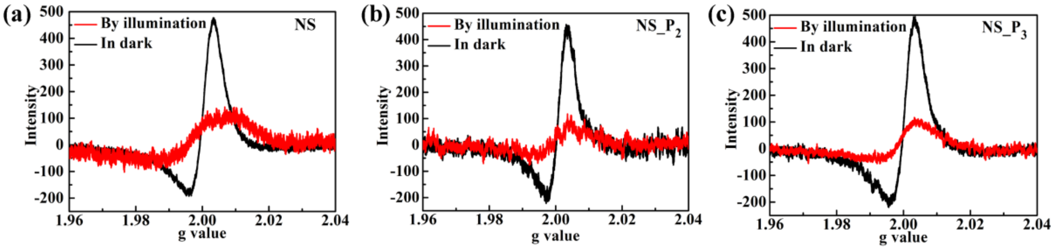

Figure S29. (a) In situ EPR spectra of NS with and without light irradiation at 0 °C. (b) In situ EPR spectra of NS_P_2 with and without light irradiation at 0 °C. (c) In situ EPR spectra of NS_P_3 with and without light irradiation at 0 °C.

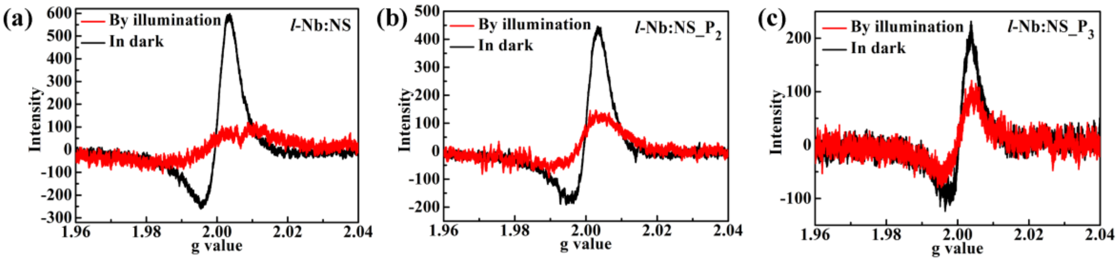

Figure S30. (a) In situ EPR spectra of *l*-Nb:NS with and without light irradiation at 0 °C. (b) In situ EPR spectra of *l*-Nb:NS_P_2 with and without light irradiation at 0 °C. (c) In situ EPR spectra of *l*-Nb:NS_P_3 with and without light irradiation at 0 °C.

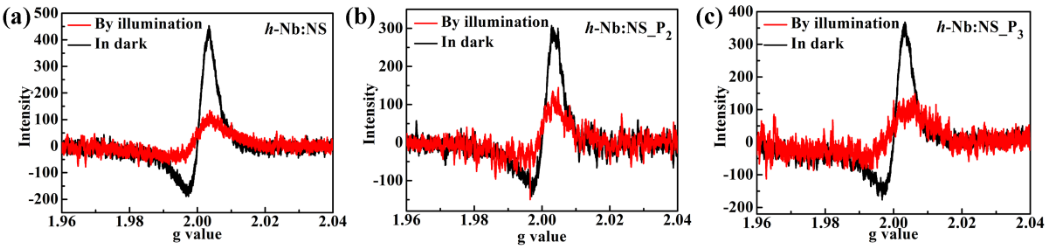

Figure S31. (a) In situ EPR spectra of *h*-Nb:NS with and without light irradiation at 0 °C. (b) In situ EPR spectra of *h*-Nb:NS_P_2 with and without light irradiation at 0 °C. (c) In situ EPR spectra of *h*-Nb:NS_P_3 with and without light irradiation at 0 °C.

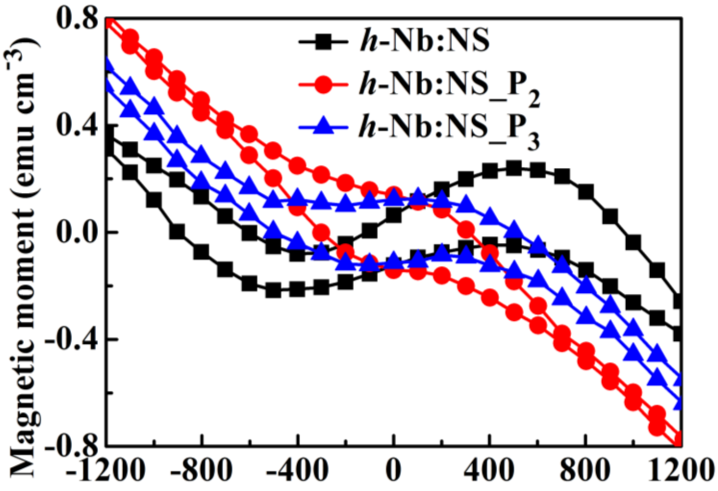

Figure S32. Room-temperature hysteresis curves of *h*-Nb:NS, *h*-Nb:NS_P_2, and *h*-Nb:NS_P_3 with applied magnetic field perpendicular to the sample surface.

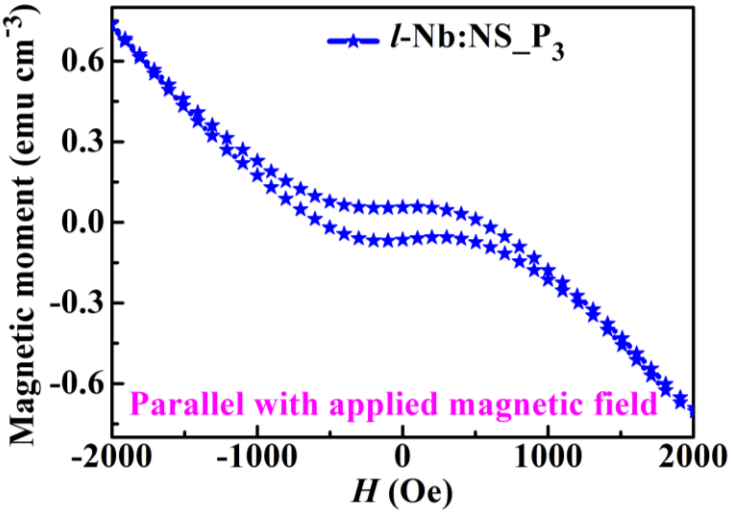

Figure S33. Room-temperature hysteresis curves of *l*-Nb:NS_P$_3$ with applied magnetic field parallel with the sample surface.

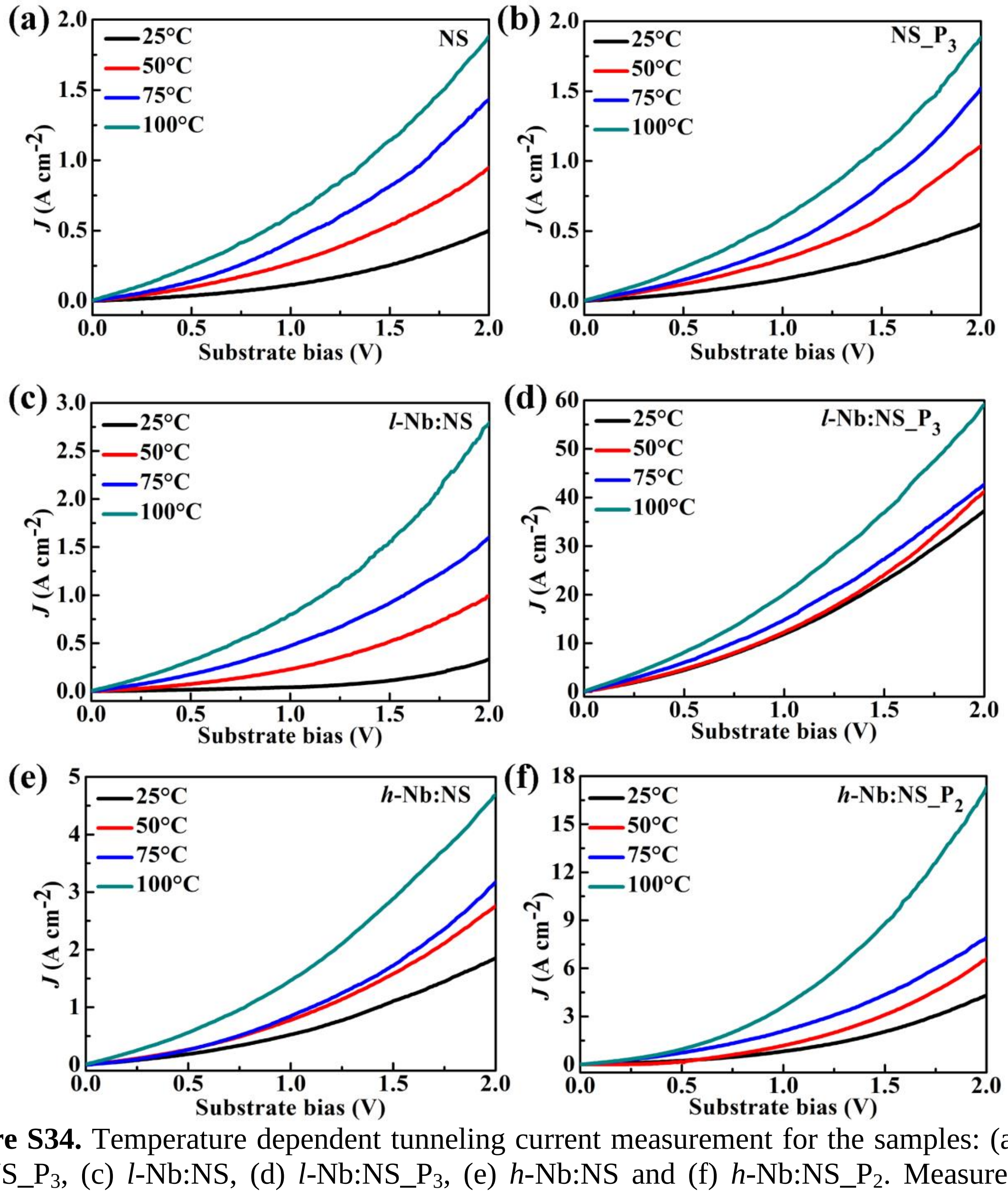

Figure S34. Temperature dependent tunneling current measurement for the samples: (a) NS, (b) NS_P$_3$, (c) *l*-Nb:NS, (d) *l*-Nb:NS_P$_3$, (e) *h*-Nb:NS and (f) *h*-Nb:NS_P$_2$. Measurements were taken at (black line) 25 °C, (red line) 50 °C, (blue line) 75 °C and (green line) 100 °C, respectively.

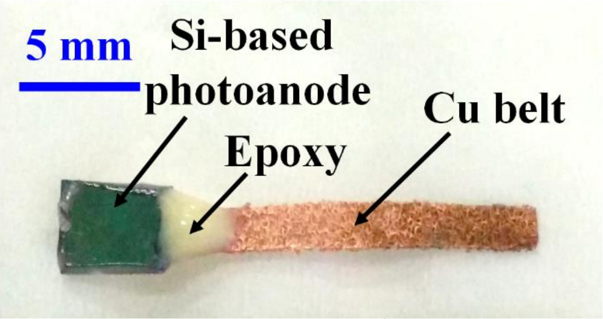

Figure S35. Photograph of *l*-Nb:NS_P$_3$ with ~0.1 cm^2 area.